Reentrant Correlated Insulators in Twisted Bilayer Graphene at 25 T (2π Flux)

Jonah Herzog-Arbeitman,[1] Aaron Chew,[1] Dmitri K. Efetov,[2] and B. Andrei Bernevig[1,3,4]
[1]Department of Physics, Princeton University, Princeton, New Jersey 08544, USA
[2]ICFO–Institut de Ciencies Fotoniques, The Barcelona Institute of Science and Technology, Castelldefels, Barcelona 08860, Spain
[3]Donostia International Physics Center, P. Manuel de Lardizabal 4, 20018 Donostia-San Sebastian, Spain
[4]IKERBASQUE, Basque Foundation for Science, Bilbao, Spain

(Received 23 November 2021; accepted 19 July 2022; published 9 August 2022)

Twisted bilayer graphene (TBG) is remarkable for its topological flat bands, which drive strongly interacting physics at integer fillings, and its simple theoretical description facilitated by the Bistritzer-MacDonald Hamiltonian, a continuum model coupling two Dirac fermions. Because of the large moiré unit cell, TBG offers the unprecedented opportunity to observe reentrant Hofstadter phases in laboratory-strength magnetic fields near 25 T. This Letter is devoted to magic angle TBG at 2π flux where the magnetic translation group commutes. We use a newly developed gauge-invariant formalism to determine the exact single-particle band structure and topology. We find that the characteristic TBG flat bands reemerge at 2π flux, but, due to the magnetic field breaking $C_{2z}\mathcal{T}$, they split and acquire Chern number ± 1. We show that reentrant correlated insulating states appear at 2π flux driven by the Coulomb interaction at integer fillings, and we predict the characteristic Landau fans from their excitation spectrum.

DOI: 10.1103/PhysRevLett.129.076401

Introduction.—Twisted bilayer graphene (TBG) is the prototypical moiré material obtained from rotating two graphene layers by an angle θ. Near the magic angle $\theta = 1.05°$, the two bands near charge neutrality flatten to a few meV, pushing the system into the strong-coupling regime featuring correlated insulators and superconductors [1–7]. Because of the large moiré unit cell, magnetic fluxes of 2π are achieved at only 25 T. In Hofstadter tight-binding models with the Peierls substitution, e.g., the square lattice, the 2π-flux and zero-flux models are equivalent, although the situation is more complicated in TBG [8]. This begs the question: do insulating and superconducting phases of TBG repeat at 25 T?

We study the Bistritzer-MacDonald (BM) Hamiltonian [9], describing the interlayer moiré-scale coupling of the graphene Dirac fermions within a single valley. We write the BM Hamiltonian [neglecting $O(\theta)$ terms] as

$$H_{\mathrm{BM}}(\mathbf{r}) = \begin{pmatrix} -i\hbar v_F \boldsymbol{\nabla}\cdot\boldsymbol{\sigma} & \text{H.c.} \\ \sum_{j=1}^{3} T_j e^{2\pi i \mathbf{q}_j\cdot\mathbf{r}} & -i\hbar v_F \boldsymbol{\nabla}\cdot\boldsymbol{\sigma} \end{pmatrix}. \quad (1)$$

Here, $\mathbf{q}_j = C_{3z}^{j-1}\mathbf{q}_1$ are the interlayer momentum hoppings, $\mathbf{q}_1 = [0, 4\sin(\theta/2)/3a_g]$, and $a_g = 0.246$ nm is the graphene lattice constant. The BM couplings $T_1 = w_0\sigma_0 + w_1\sigma_1$, $T_{j+1} = \exp[(2\pi i/3)j\sigma_3]T_1\exp[-(2\pi i/3)j\sigma_3]$ act on the sublattice indices of the Dirac fermions, and σ_j are the Pauli matrices. The lattice potential scale is $w_1 = 110$ meV with $w_0/w_1 = 0.6$–0.8 [10,11] and the kinetic energy scale is $2\pi\hbar v_F|\mathbf{q}_1| = 190$ meV. The spectrum of $H_{\mathrm{BM}}(\mathbf{r})$ has been thoroughly investigated [12–17].

The salient feature of the BM model from the Hofstadter perspective is the size of the moiré unit cell. After a unitary transform by $\mathrm{diag}(e^{i\pi\mathbf{q}_1\cdot\mathbf{r}}, e^{-i\pi\mathbf{q}_1\cdot\mathbf{r}})$, $H_{\mathrm{BM}}(\mathbf{r})$ is put into Bloch form and is periodic under translations by $\mathbf{a}_i$, the moiré lattice vectors [18]. Near the magic angle, the moiré unit cell area $\Omega = |\mathbf{a}_1 \times \mathbf{a}_2|$ is a factor of $\theta^{-2} \sim 3000$ times larger than the graphene unit cell. This dramatic increase in size brings the Hofstadter regime

$$\phi = eB\Omega/\hbar \sim 2\pi \quad (2)$$

within reach, showcasing physics which is only possible in strong flux [8,19–24]. Here, $e/2\pi\hbar$ is the flux quantum (henceforth $e = \hbar = 1$) and the magnetic field B is near 25 T at $\phi = 2\pi$ and $\theta = 1.05°$. Although there is not an exact 2π periodicity in flux, we will show that the flat bands and correlated insulators are revived at $\phi = 2\pi$.

A constant magnetic field $\epsilon_{ij}\partial_i A_j = B > 0$ (repeated indices are summed) is incorporated into Eq. (1) via the canonical substitution $-i\boldsymbol{\nabla} \to \boldsymbol{\pi} = -i\boldsymbol{\nabla} - \mathbf{A}(\mathbf{r})$ yielding H_{BM}^{ϕ}. Because $\mathbf{A}(\mathbf{r})$ breaks translation symmetry, the spectrum in flux cannot be solved using Bloch's theorem. This problem has a long history with many approaches [25–38], most frequently relying on the Landau gauge. However, an understanding of TBG in flux requires more than just the spectrum. To rigorously derive expressions for the Wilson loop and many-body form factors at 2π flux, we employ a newly developed gauge-invariant formalism [39] built from the magnetic translation group. We apply the theory here to study the single-particle and many-body

physics of TBG at 2π flux. Accompanying this Letter, Ref. [40] exppaper experimentally confirms our prediction of reentrant correlated insulators at 2π flux.

Magnetic Bloch theorem.—In zero flux, the translation group of a crystal allows one to construct an orthonormal basis of momentum eigenstates labeled by $\mathbf{k}$ in the Brillouin zone and the spectrum is given by the Bloch Hamiltonian at each $\mathbf{k}$. A similar construction can be followed at 2π flux where the magnetic translation group commutes and is isomorphic to the zero-flux translation group. As detailed in Ref. [39], we construct irreps at $\phi = 2\pi$, valid in any gauge, in the form

$$|\mathbf{k}, n, \alpha, l\rangle = \frac{1}{\sqrt{\mathcal{N}(\mathbf{k})}} \sum_{\mathbf{R}} e^{-i\mathbf{k}\cdot\mathbf{R}} T_{\mathbf{a}_1}^{\mathbf{R}\cdot\mathbf{b}_1} T_{\mathbf{a}_2}^{\mathbf{R}\cdot\mathbf{b}_2} |n, \alpha, l\rangle, \tag{3}$$

where $\mathbf{R}$ is the moiré Bravais lattice, $\alpha = 1, \ldots, 4$ is the composite sublattice-layer index, and n is the Landau level defined by $|n, \alpha\rangle = (a^{\dagger n}/\sqrt{n!})|0, \alpha\rangle$, $a|0, \alpha\rangle = 0$ with a, $a^\dagger$ the Landau level operators [40]. The states in Eq. (3) are orthogonal, periodic, and obey $T_{\mathbf{a}_i}|\mathbf{k}, n, \alpha\rangle = e^{i\mathbf{k}\cdot\mathbf{a}_i}|\mathbf{k}, n, \alpha\rangle$ where $T_{\mathbf{a}_i}$ are the magnetic translation operators at 2π flux. The normalization $\mathcal{N}(\mathbf{k})$ can be expressed in terms of theta functions [40] and is responsible for encoding the topology of the underlying Landau levels in momentum space. With the basis states in Eq. (3), we can diagonalize the Hamiltonian at each $\mathbf{k}$ to produce a band structure. As computed in Fig. 1(a), the famous flat bands of magic angle TBG reappear at 2π flux. We use the open momentum space technique [38] to obtain the Hofstadter spectrum [Fig. 1(b)] which shows the evolution of the higher energy passive bands. Despite splitting into Hofstadter bands at rational flux, the density of states remains strongly confined all the way up to 2π flux where full density Bloch-like flat bands reemerge.

Topology of the flat bands.—Similar to the zero flux TBG flat bands, the reentrant flat bands at 2π flux have a very small bandwidth of $\sim$1 meV. However, their topology is quite different due to the breaking of crystalline symmetries by magnetic field. Let us review the zero flux model. Reference [12] showed that the space group $p6'2'2$ of the BM Hamiltonian [Eq. (1)] was generated by C_{3z}, C_{2x}, and $C_{2z}\mathcal{T}$ and also featured an approximate unitary particle-hole operator P. Notably, $C_{2z}\mathcal{T}$ alone is sufficient to protect the gapless Dirac points and fragile topology of the flat bands [12]. Because a perpendicular magnetic field is reversed by time-reversal and C_{2x} (while it is invariant under in-plane rotations), C_{2x} and $C_{2z}\mathcal{T}$ are broken for all nonzero flux [8]. Thus, the space group of H_{BM}^{ϕ} is reduced to $p31m'$ which is generated by C_{3z} and $M\mathcal{T} \equiv C_{2x}C_{2z}\mathcal{T}$. P also remains a symmetry.

Without $C_{2z}\mathcal{T}$, the system changes substantially. The most direct way to assess the topology at 2π flux is to calculate the non-Abelian Wilson loop. To do so, we need an expression for the Berry connection $\mathcal{A}^{MN}(\mathbf{k})$ where M, N index the occupied bands. At 2π flux, the Berry connection $\mathcal{A}_i = \mathbf{b}_i \cdot \mathcal{A}$ contains new contributions [39]:

$$\mathcal{A}_i^{MN}(\mathbf{k}) = [U^\dagger(\mathbf{k})(i\partial_{k_i} - \epsilon_{ij}\tilde{Z}_j)U(\mathbf{k})]^{MN} - \delta^{MN}\epsilon_{ij}\partial_{k_j} \log\sqrt{\mathcal{N}(\mathbf{k})}, \tag{4}$$

where $\mathrm{U}(\mathbf{k})$ is a matrix whose columns are the flat band eigenvectors. The Abelian term in the second line of Eq. (4) is an exact expression for the Berry connection of a Landau level and accounts for the Chern number of the basis states [39]. The non-Abelian term $\tilde{Z}_j$ acts on the Landau level indices [40]. We numerically calculate the Wilson loop [41] over the flat bands in Fig. 1(c) which shows no winding (see Ref. [40] for the Wilson loops of the dispersive bands). Hence, the fragile topology of the flat bands is trivialized by flux. This is possible without a gap closing because the fragile topology of TBG is reliant on $C_{2z}\mathcal{T}$ [12,15,42–44], which is broken by flux. The total Chern number of the flat bands is zero, so they cannot be modeled as Landau levels despite the strong flux.

To gain a deeper understanding of the topology at 2π flux, we study the band representation $\mathcal{B}$ with topological quantum chemistry [45–47]. First, Fig. 1(b) demonstrates that the flat bands remain gapped from all other bands in

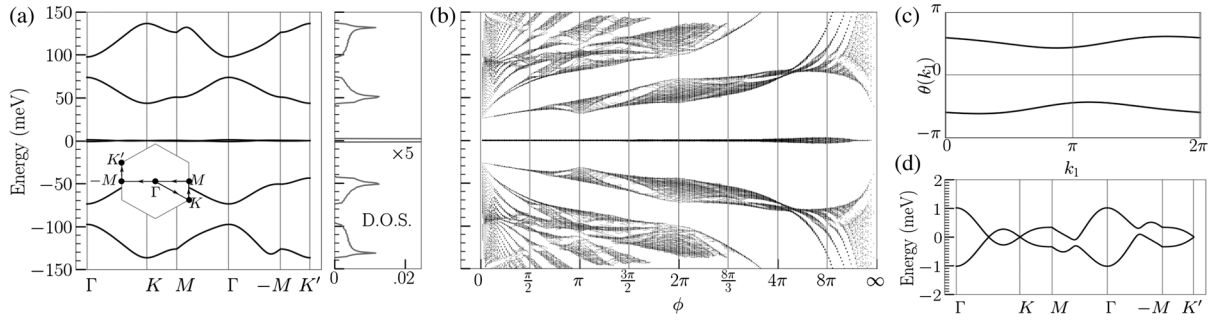

FIG. 1. TBG in flux. (a) The band structure and density of states at $\phi = 2\pi$, $w_0/w_1 = 0.8$, and $\theta = 1.05°$ reveal $\sim$1.5 meV flat bands with a 40 meV gap. (b) The Hofstadter spectrum shows the flat bands remain gapped at all flux. (c) The Wilson loop of the two flat bands is trivial due to $C_2\mathcal{T}$ breaking when particle-hole symmetry is intact. (d) The flat bands at 2π flux.

flux (despite the fragile topology of TBG [8]). Thus, $\mathcal{B}$ can be obtained by reducing the band representation of TBG in zero flux derived in Ref. [12] to $p31m'$. We find

$$\mathcal{B} = 2\Gamma_1 + K_2 + K_3 + K_2' + K_3' = A_{2b} \uparrow p31m', \quad (5)$$

which is an elementary band representation and is not topological. The irreps are defined by

$$\begin{array}{c|cc} 3m' & 1 & C_{3z} \\ \hline \Gamma_1 & 1 & 1 \end{array}, \quad \begin{array}{c|cc} 3 & 1 & C_{3z} \\ \hline K_2 & 1 & e^{\frac{2\pi i}{3}} \\ K_3 & 1 & e^{-\frac{2\pi i}{3}} \end{array}, \quad \begin{array}{c|cc} 3 & 1 & C_{3z} \\ \hline K_3' & 1 & e^{\frac{2\pi i}{3}} \\ K_2' & 1 & e^{-\frac{2\pi i}{3}} \end{array} \quad (6)$$

and A_{2b} denotes two irreps of s orbitals at the corners of the moiré unit cell, matching the charge centers at zero flux [10,12,48]. Consulting the `BilbaoCrystallographicServer`, we observe that Eq. (5) is decomposable in momentum space [49–51]. Hence, the reduced symmetry group in flux permits the flat bands to be split into disconnected Chern bands given by

$$\mathcal{B} = \mathcal{B}_+ + \mathcal{B}_- = (\Gamma_1 + K_2 + K_3') + (\Gamma_1 + K_3 + K_2'), \quad (7)$$

where $\mathcal{B}_\pm$ carries Chern number $C = \pm 1 \bmod 3$ [52]. The irreps of $\mathcal{B}_\pm$ at the K and K' points are related by the antiunitary operator $M\mathcal{T}$ which obeys $C_{3z}M\mathcal{T} = M\mathcal{T}C_{3z}^\dagger$, so Eq. (7) is the only allowed decomposition. We show below that the addition of P, which is not part of the irrep classification (it is not a crystallographic symmetry), forbids this splitting. To split the flat bands, we incorporate the exact θ dependence into the kinetic terms of Eq. (1), breaking P [12,15] and opening a $\sim$0.5 meV gap at K and K'. We verify the Chern number decomposition in Eq. (7) from the Wilson loop [40].

Equation (7) suggests a remarkable similarity to the topology of the flat bands at zero flux, where $C_{2z}\mathcal{T}$ enforces *connected* bands with opposite Chern numbers [12,15,42,43]. We have shown that flux breaks $C_{2z}\mathcal{T}$ and allows the bands to split, yielding strong topology. The flat bands at 2π flux carry opposite Chern numbers, but they cannot annihilate with each other: $M\mathcal{T}$ symmetry ensures any band touching come in pairs so the Chern numbers can only change in multiples of two.

The particle-hole approximation in Eq. (1) prevents the Chern decomposition in Eq. (7) because P and C_{3z} enforce gapless points at K and K' as we now show. Observe that the K and K' points are symmetric under the anticommuting symmetry $\mathcal{P} = PM\mathcal{T}$ because P takes $\mathbf{k} \to -\mathbf{k}$ and $M\mathcal{T}$ takes $(k_x, k_y) \to (k_x, -k_y)$ [12]. $\mathcal{P}$ is antiunitary and obeys $C_{3z}\mathcal{P} = \mathcal{P}C_{3z}^\dagger$. As such, a state $|\omega\rangle$ of energy $E \neq 0$ and C_{3z} eigenvalue ω ensures a distinct state $\mathcal{P}|\omega\rangle$ with C_{3z} eigenvalue ω and energy $-E$. Thus, all states at $E \neq 0$ come in $\mathcal{P}$-related pairs with the same C_{3z} eigenvalue. Hence, if $\mathcal{P}$ is unbroken, the irreps of $\mathcal{B}$ at K and K' are pinned together at $E = 0$ because they have different C_{3z} eigenvalues.

Coulomb ground states.—Flat bands provide a tractable many-body problem because exact ground states can be obtained for the interaction term while reliably neglecting the competing effects of the kinetic energy after projection [53]. Band topology plays an essential role in this setting. The unprojected Coulomb interaction consists of commuting local operators, but projecting into the flat bands introduces nontriviality due to the wave function form factors with a profound effect on the charge excitations [54]. The preceding sections have established TBG at 2π flux as a flat band system with different topology in its wave functions due to the breaking of $C_{2z}\mathcal{T}$, serving as a useful comparison to TBG at zero flux.

We now study many-body states where the spin and valley degrees of freedom are important. The low energy states come from the two graphene valleys which we index by $\eta = \pm 1$. The valleys are interchanged by C_{2z} which is unbroken by flux, and hence the flat bands are each fourfold degenerate. To split the degeneracy, we consider adding the interaction

$$H_{\text{int}} = \frac{1}{2\Omega_{\text{tot}}} \sum_{\mathbf{q}} V(\mathbf{q}) \bar{\rho}_{-\mathbf{q}} \bar{\rho}_{\mathbf{q}}, \qquad \bar{\rho}_{\mathbf{q}} = \int d^2 r \, e^{-i\mathbf{q}\cdot\mathbf{r}} \bar{n}(\mathbf{r}), \quad (8)$$

where $V(\mathbf{q}) > 0$ is the screened Coulomb potential [55,56], $\bar{n}(\mathbf{r})$ is the total electron density (summed over valley and spin) measured from charge neutrality, and Ω_{tot} is the area of the sample. In zero flux, the Hamiltonian conserves spin, charge, and valley, so there is an exact $\mathrm{U}(2) \times \mathrm{U}(2)$ symmetry. It is natural to work in a strong coupling expansion where we project H_{int} onto the two flat bands and neglect their kinetic energy (including particle-hole breaking terms) entirely. This is a very reliable approximation because the bandwidth is $\sim$1 meV and the interaction strength is $\sim$20 meV. In this limit, $C_{2z}P$ commutes with the projected H_{int} operator and the symmetry group is promoted to U(4) [55,57].

We now discuss the fate of the U(4) symmetry in flux. At $B \sim 25$ T, the Zeeman effect shifts the energy of the spin $\pm 1/2$ electrons by $\pm\mu_B B = \pm 1.4$ meV where μ_B is the Bohr magneton. This shift is comparable to the bandwidth, so it is consistent to neglect both at leading order. [The Zeeman term will choose the spin-polarized states out of the U(4) manifold.] We should also consider twist angle homogeneity which has recently come under scrutiny [58–60]. Experiments indicate that even in high quality devices, the moiré twist angle θ varies locally up to 0.1° [61–63], leading to local variations in the unit cell and hence the flux. In a realistic sample with domains of varying θ at constant B, we expect deviations from the 2π flux flat band wave functions. However, the large interaction strength and gap to the passive bands still makes the strong coupling expansion appropriate.

An analytic study of the strong-coupling problem is possible because H_{int} is positive semidefinite [53].

Following Ref. [54], we study exact eigenstates at fillings $\nu = 0,\ 2,\ 4$ ($-\nu$ follows from many-body particle-hole symmetry [55]) and derive the excitation spectrum, effectively determining the complete renormalization of the flat bands by the Coulomb interaction. Reference [54] was also able to study odd ν perturbatively using the chiral symmetry at $w_0 = 0$ [13,14,16,64]. The chiral limit at 2π flux is topologically distinct [64] from the physical regime $w_0/w_1 = 0.6 - 0.8$ (unlike at zero flux) so this approach is inapplicable. Odd fillings are left to future work.

The many-body calculation at 2π flux is tractable using a gauge-invariant expression for H_{int} and the form factors. Following Ref. [65], we produce exact many-body insulator eigenstates of the projected H_{int} at even ν:

$$|\Psi_\nu\rangle = \prod_{\mathbf{k}} \prod_{j}^{(4+\nu)/2} \gamma^\dagger_{\mathbf{k},+,\eta_j,s_j} \gamma^\dagger_{\mathbf{k},-,\eta_j,s_j} |0\rangle, \tag{9}$$

where $\gamma^\dagger_{\mathbf{k},M,\eta,s}$ creates a state at momentum $\mathbf{k}$, valley η, and spin s in the $M = \pm 1$ band. The states $|\Psi_\nu\rangle$ fully occupy the two flat bands for arbitrary η_j, s_j forming a U(4) multiplet. Including valley and spin, there are eight flat bands; $|\Psi_\nu\rangle$ fills $(4+\nu)/2$ of them. At $\nu = 0$, $|\Psi_0\rangle$ must be a ground state because H_{int} is positive semidefinite and $H_{\text{int}}|\Psi_0\rangle = 0$. At $\nu = \pm 4$ where the system is a band insulator, $|\Psi_{\pm 4}\rangle$ are trivially ground states because they are completely empty or occupied. The $|\Psi_{\pm 2}\rangle$ states are exact eigenstates, and we argue they are ground states using the flat metric condition (FMC) [65] which assumes the Hartree potential of the flat bands is trivial. Reference [55] found that the FMC holds reliably at zero flux, and we check that the FMC is similarly reliable at 2π flux [39]. Like at zero flux, $|\Psi_\nu\rangle$ has Chern number zero, but without $C_{2z}\mathcal{T}$ there is no fragile topology.

Charge excitations.—The exact eigenstates $|\Psi_\nu\rangle$ enable us to compute the charge excitation spectrum at filling ν. The Hamiltonian $R^\eta_+(\mathbf{k})$ governing the $+1$ charge spectrum is defined

$$[H_{\text{int}} - \mu N, \gamma^\dagger_{\mathbf{k},M,s,\eta}]|\Psi_\nu\rangle \equiv \frac{1}{2}\sum_N \gamma^\dagger_{\mathbf{k},N,s,\eta} [R^\eta_+(\mathbf{k})]_{NM} |\Psi_\nu\rangle, \tag{10}$$

where η, s are *unoccupied* indices in $|\Psi_\nu\rangle$ and μ is the chemical potential [40]. Counting the flavors in Eq. (9), at filling ν the charge ± 1 excitations come in multiples of $(4 \mp \nu)/2$. A direct calculation of $R^\eta_\pm(\mathbf{k})$, the ± 1 charge excitation Hamiltonian, is possible thanks to our gauge-invariant expression for the form factors in flux. Performing the commutators at $\nu = 0$ in Eq. (10) gives [40]

$$R_+(\mathbf{k}) = \sum_{\mathbf{q}} \frac{V(\mathbf{q})}{\Omega_{\text{tot}}} M^\dagger(\mathbf{k},\mathbf{q}) M(\mathbf{k},\mathbf{q}) \tag{11}$$

and the form factor matrices in the flat bands are

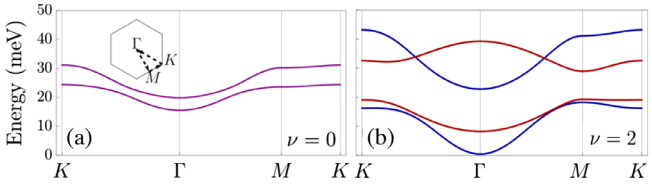

FIG. 2. $\frac{1}{2}R^\eta_\pm(\mathbf{k})$ spectra at $w_0/w_1 = 0.71$. (a) At $\nu = 0$, the charge ± 1 excitations are identical and feature a quadratic (massive) dispersion at the Γ point. (b) At $\nu = 2$, the charge -1 excitation (red) has a large mass, strongly suppressing the Landau fans pointing toward charge neutrality, while the $+1$ excitation (blue) is lighter by a factor of 3. The $+1$ charge gap at $\nu = 2$ is $\sim$0.5 meV or roughly 5 K.

$$M(\mathbf{k},\mathbf{q}) = e^{i\xi_{\mathbf{q}}(\mathbf{k})} U^\dagger(\mathbf{k}-\mathbf{q}) \mathcal{H}^{\mathbf{q}} U(\mathbf{k}), \tag{12}$$

where $\mathcal{H}^{\mathbf{q}} = e^{i\epsilon_{ij} q_i \tilde{Z}_j}$ is a unitary matrix acting on the Landau level indices like in the Berry connection [see Eq. (4)] and $e^{i\xi_{\mathbf{q}}(\mathbf{k})}$ can be expressed in terms of Siegel theta functions [40]. Equation (11) demonstrates that the excitations at $\nu = 0$ are governed by the wave functions $\mathrm{U}(\mathbf{k})$ (like at zero flux) as well as $\mathcal{H}^{\mathbf{q}}$, a new factor intrinsic to magnetic flux. The phase factor $e^{i\xi_{\mathbf{q}}(\mathbf{k})}$ cancels in Eq. (11) at $\nu = 0$, but contributes nontrivially at $\nu = \pm 2$ [40]. Next, because $V(\mathbf{q}) > 0$ and $M^\dagger M$ is a positive definite matrix, we see that $R_\pm(\mathbf{k})$ is positive definite and thus describes gapped excitations (an insulator). Lastly, we observe that all $\mathbf{k}$ dependence in $R_\pm(\mathbf{k})$ comes from the wave functions, so the dispersion of the excitation bands depends the nontriviality of $\mathrm{U}(\mathbf{k})$. For example, in the decoupled Landau limit where $\mathrm{U}(\mathbf{k})$ is independent of $\mathbf{k}$ and nonzero only for a single Landau level n, $R_\pm(\mathbf{k})$ has exactly flat bands. We plot the excitation spectrum at $\nu = 0$ and $\nu = 2$ in Fig. 2, observing significant dispersion since, as shown by irreps Eq. (5), TBG at 2π flux is far from the Landau level regime.

The dispersion of the excitations leaves distinctive signatures in the Landau fans emanating from the $|\Psi_\nu\rangle$ insulators [11,29,66]. At $\nu = 0$, the ± 1 charge excitations are identical and their dispersion features a charge gap to a band with a quadratic minima at the Γ point. Hence, at low densities, there are $(4 \mp 0)/2 = 2$ massive quasiparticles, counting the degenerate charge excitations in different spin-valley flavors. As the flux is increased, the massive quadratic excitations form Landau levels (quantum Hall states), leading to Landau fans away from $\nu = 0$ in multiples of 2—half the Landau level degeneracy of TBG near $B = 0$. The gap between the two excitation bands at Γ depends on w_0/w_1. Figure 2(a) shows the generic case at $w_0/w_1 = 0.71$, but at $w_0/w_1 = 0.8$ the two bands are nearly degenerate at Γ [40]. At $\nu = 2$, the -1 excitation (toward charge neutrality) has a large mass which reduces the gap between Landau levels and masks would-be insulating states. However, the $+1$ excitation has a smaller effective mass and will create Landau levels in multiples of

$(4-2)/2=1$. We do not discuss excitations above $\nu=4$ here because they fill the passive bands, and we check that the charge -1 excitation below $\nu=4$ (not shown) is gapped with a very large mass. We note that at zero flux with $C_{2z}\mathcal{T}$, the excitation bands must be degenerate at the Γ point [54,67]. Based on the U(4) symmetry which determines the $(4\mp\nu)/2$ degeneracy of the excitations, the breaking of $C_{2z}\mathcal{T}$ which allows the bands to be gapped at Γ, and the large mass of excitations toward charge neutrality, we predict the Landau fans emerging from $\nu=0$ and $\nu=2$ away from charge neutrality to have degeneracies 2 and 1, respectively.

Discussion.—We used an exact method to study TBG at 2π flux, yielding comprehensive results for the single-particle and many-body physics. Recently, interest in reentrant superconductivity and correlated phases in strong flux has invigorated research in moiré materials [68–70]. Our formalism makes it possible to study such phenomena with the tools of modern band theory and without recourse to approximate models. We find that the emblematic topological flat bands and correlated insulators of TBG are reentrant at $\phi=2\pi$, providing strong evidence that magic-angle physics recurs at ~25 T. The excitation spectrum at $\nu=2$ reveals dispersive quasiparticles away from charge neutrality as at zero flux (but with half the degeneracy due to $C_{2z}\mathcal{T}$ breaking). This leads us to conjecture that superconductivity, which occurs at $\phi=0$ upon doping correlated insulating states, may also be reentrant at 2π flux [71].

We thank Zhi-Da Song for early insight and Luis Elcoro for useful discussions. B. A. B. and A. C. were supported by the ONR Grant No. N00014-20-1-2303, DOE Grant No. DESC0016239, the Schmidt Fund for Innovative Research, Simons Investigator Grant No. 404513, the Packard Foundation, the Gordon and Betty Moore Foundation through Grant No. GBMF8685 toward the Princeton theory program, and a Guggenheim Fellowship from the John Simon Guggenheim Memorial Foundation. Further support was provided by the NSF-MRSEC Grants No. DMR-1420541 and No. DMR-2011750, BSF Israel U.S. Foundation Grant No. 2018226, and the Princeton Global Network Funds. J. H. A. is supported by a Marshall Scholarship funded by the Marshall Aid Commemoration Commission.

Note added.—Recently, Ref. [72] appeared which investigated reentrant single-particle flat bands in TBG using a tight-binding model on very large commensurate unit cell. Their findings are consistent with our continuum approach when both valleys are included.

[1] Yuan Cao, Valla Fatemi, Ahmet Demir, Shiang Fang, Spencer L. Tomarken, Jason Y. Luo, Javier D. Sanchez-Yamagishi, Kenji Watanabe, Takashi Taniguchi, Efthimios Kaxiras, Ray C. Ashoori, and Pablo Jarillo-Herrero, Correlated insulator behaviour at half-filling in magic-angle graphene superlattices, Nature (London) **556**, 80 (2018).

[2] Yuan Cao, V. Fatemi, S. Fang, K. Watanabe, T. Taniguchi, E. Kaxiras, and P. Jarillo-Herrero, Unconventional superconductivity in magic-angle graphene superlattices, Nature (London) **556**, 43 (2018).

[3] Kyounghwan Kim, Ashley DaSilva, Shengqiang Huang, Babak Fallahazad, Stefano Larentis, Takashi Taniguchi, Kenji Watanabe, Brian J. LeRoy, Allan H. MacDonald, and Emanuel Tutuc, Tunable moiré bands and strong correlations in small-twist-angle bilayer graphene, Proc. Natl. Acad. Sci. U.S.A. **114**, 3364 (2017).

[4] Dante M. Kennes, Martin Claassen, Lede Xian, Antoine Georges, Andrew J. Millis, James Hone, Cory R. Dean, D. N. Basov, Abhay N. Pasupathy, and Angel Rubio, Moiré heterostructures as a condensed-matter quantum simulator, Nat. Phys. **17**, 155 (2021).

[5] Leon Balents, Cory R. Dean, Dmitri K. Efetov, and Andrea F. Young, Superconductivity and strong correlations in moiré flat bands, Nat. Phys. **16**, 725 (2020).

[6] Jianpeng Liu and Xi Dai, Orbital magnetic states in moiré graphene systems, Nat. Rev. Phys. **3**, 367 (2021).

[7] Yanbang Chu, Le Liu, Yalong Yuan, Cheng Shen, Rong Yang, Dongxia Shi, Wei Yang, and Guangyu Zhang, A review of experimental advances in twisted graphene moiré superlattice, Chin. Phys. B **29**, 128104 (2020).

[8] Jonah Herzog-Arbeitman, Zhi-Da Song, Nicolas Regnault, and B. Andrei Bernevig, Hofstadter Topology: Noncrystalline Topological Materials at High Flux, Phys. Rev. Lett. **125**, 236804 (2020).

[9] Rafi Bistritzer and Allan H. MacDonald, Moiré bands in twisted double-layer graphene, Proc. Natl. Acad. Sci. U.S.A. **108**, 12233 (2011).

[10] Mikito Koshino, Noah F. Q. Yuan, Takashi Koretsune, Masayuki Ochi, Kazuhiko Kuroki, and Liang Fu, Maximally Localized Wannier Orbitals and the Extended Hubbard Model for Twisted Bilayer Graphene, Phys. Rev. X **8**, 031087 (2018).

[11] Ipsita Das, Xiaobo Lu, Jonah Herzog-Arbeitman, Zhi-Da Song, Kenji Watanabe, Takashi Taniguchi, B. Andrei Bernevig, and Dmitri K. Efetov, Symmetry-broken Chern insulators and Rashba-like Landau-level crossings in magic-angle bilayer graphene, Nat. Phys. **17**, 710 (2021).

[12] Zhi-Da Song, Zhijun Wang, Wujun Shi, Gang Li, Chen Fang, and B. Andrei Bernevig, All Magic Angles in Twisted Bilayer Graphene are Topological, Phys. Rev. Lett. **123**, 036401 (2019).

[13] Grigory Tarnopolsky, Alex Jura Kruchkov, and Ashvin Vishwanath, Origin of Magic Angles in Twisted Bilayer Graphene, Phys. Rev. Lett. **122**, 106405 (2019).

[14] B. Andrei Bernevig, Zhi-Da Song, Nicolas Regnault, and Biao Lian, Twisted bilayer graphene. I. Matrix elements, approximations, perturbation theory, and a $k\cdot p$ two-band model, Phys. Rev. B **103**, 205411 (2021).

[15] Zhi-Da Song, Biao Lian, Nicolas Regnault, and B. Andrei Bernevig, Twisted bilayer graphene. II. Stable symmetry anomaly, Phys. Rev. B **103**, 205412 (2021).

[16] Jie Wang, Yunqin Zheng, Andrew J. Millis, and Jennifer Cano, Chiral approximation to twisted bilayer graphene: Exact intravalley inversion symmetry, nodal structure, and

implications for higher magic angles, Phys. Rev. Research **3**, 023155 (2021).
[17] Bin-Bin Chen, Yuan Da Liao, Ziyu Chen, Oskar Vafek, Jian Kang, Wei Li, and Zi Yang Meng, Realization of topological Mott insulator in a twisted bilayer graphene lattice model, Nat. Commun. **12**, 5480 (2021).
[18] Liujun Zou, Hoi Chun Po, Ashvin Vishwanath, and T. Senthil, Band structure of twisted bilayer graphene: Emergent symmetries, commensurate approximants, and Wannier obstructions, Phys. Rev. B **98**, 085435 (2018).
[19] Douglas R. Hofstadter, Energy levels and wave functions of Bloch electrons in rational and irrational magnetic fields, Phys. Rev. B **14**, 2239 (1976).
[20] Jian Wang and Luiz H. Santos, Classification of Topological Phase Transitions and van Hove Singularity Steering Mechanism in Graphene Superlattices, Phys. Rev. Lett. **125**, 236805 (2020).
[21] C. Albrecht, J. H. Smet, K. von Klitzing, D. Weiss, V. Umansky, and H. Schweizer, Evidence of Hofstadter's Fractal Energy Spectrum in the Quantized Hall Conductance, Phys. Rev. Lett. **86**, 147 (2001).
[22] B. Andrei Bernevig and Taylor L. Hughes, *Topological Insulators and Topological Superconductors* (Princeton University Press, Princeton, New Jersey, 2013), ISBN 9780691151755.
[23] Xiaobo Lu, Biao Lian, Gaurav Chaudhary, Benjamin A. Piot, Giulio Romagnoli, Kenji Watanabe, Takashi Taniguchi, Martino Poggio, Allan H. MacDonald, B. Andrei Bernevig, and Dmitri K. Efetov, Fingerprints of fragile topology in the Hofstadter spectrum of twisted bilayer graphene close to the second magic angle, Proc. Natl. Acad. Sci. U.S.A. **118**, e2100006118 (2021).
[24] C. R. Dean, L. Wang, P. Maher, C. Forsythe, F. Ghahari, Y. Gao, J. Katoch, M. Ishigami, P. Moon, M. Koshino, T. Taniguchi, K. Watanabe, K. L. Shepard, J. Hone, and P. Kim, Hofstadter's butterfly and the fractal quantum Hall effect in moiré superlattices, Nature (London) **497**, 598 (2013).
[25] J. Zak, Magnetic translation group, Phys. Rev. **134**, A1602 (1964).
[26] J. Zak, Magnetic translation group. II. Irreducible representations, Phys. Rev. **134**, A1607 (1964).
[27] E. Brown, Aspects of group theory in electron dynamics, Solid State Phys. **22**, 313 (1969).
[28] P Streda, Theory of quantised Hall conductivity in two dimensions, J. Phys. C **15**, L717 (1982).
[29] G. H. Wannier, A result not dependent on rationality for Bloch electrons in a magnetic field, Phys. Status Solidi B **88**, 757 (1978).
[30] Daniela Pfannkuche and Rolf R. Gerhardts, Theory of magnetotransport in two-dimensional electron systems subjected to weak two-dimensional superlattice potentials, Phys. Rev. B **46**, 12606 (1992).
[31] Tong-zhong Li, Ke-lin Wang, and Jin-long Yang, Thermal properties of a two-dimensional electron gas under a one-dimensional periodic magnetic field, J. Phys. Condens. Matter **9**, 9299 (1997).
[32] J. Milton Pereira, F. M. Peeters, and P. Vasilopoulos, Landau levels and oscillator strength in a biased bilayer of graphene, Phys. Rev. B **76**, 115419 (2007).
[33] Di Xiao, Ming-Che Chang, and Qian Niu, Berry phase effects on electronic properties, Rev. Mod. Phys. **82**, 1959 (2010).
[34] Godfrey Gumbs, Desiré Miessein, and Danhong Huang, Effect of magnetic modulation on Bloch electrons on a two-dimensional square lattice, Phys. Rev. B **52**, 14755 (1995).
[35] R. Bistritzer and A. H. MacDonald, Moiré butterflies in twisted bilayer graphene, Phys. Rev. B **84**, 035440 (2011).
[36] Kasra Hejazi, Chunxiao Liu, and Leon Balents, Landau levels in twisted bilayer graphene and semiclassical orbits, Phys. Rev. B **100**, 035115 (2019).
[37] J. A. Crosse, Naoto Nakatsuji, Mikito Koshino, and Pilkyung Moon, Hofstadter butterfly and the quantum Hall effect in twisted double bilayer graphene, Phys. Rev. B **102**, 035421 (2020).
[38] Biao Lian, Fang Xie, and B. Andrei Bernevig, Open momentum space method for the Hofstadter butterfly and the quantized Lorentz susceptibility, Phys. Rev. B **103**, L161405 (2021).
[39] Jonah Herzog-Arbeitman, Aaron Chew, and B. Andrei Bernevig, Magnetic Bloch theorem and reentrant flat bands in twisted bilayer graphene at 2π flux, arXiv:2206.07717.
[40] See Supplemental Material at http://link.aps.org/supplemental/10.1103/PhysRevLett.129.076401 for a description of additional calculations.
[41] A. Alexandradinata, Xi Dai, and B. Andrei Bernevig, Wilson-loop characterization of inversion-symmetric topological insulators, Phys. Rev. B **89**, 155114 (2014).
[42] Jianpeng Liu, Junwei Liu, and Xi Dai, Pseudo Landau level representation of twisted bilayer graphene: Band topology and implications on the correlated insulating phase, Phys. Rev. B **99**, 155415 (2019).
[43] J. Ahn, S. Park, and B.-J. Yang, Failure of Nielsen-Ninomiya Theorem and Fragile Topology in Two-Dimensional Systems with Space-Time Inversion Symmetry: Application to Twisted Bilayer Graphene at Magic Angle, Phys. Rev. X **9**, 021013 (2019).
[44] Adrien Bouhon, Annica M. Black-Schaffer, and Robert-Jan Slager, Wilson loop approach to fragile topology of split elementary band representations and topological crystalline insulators with time-reversal symmetry, Phys. Rev. B **100**, 195135 (2019).
[45] Barry Bradlyn, L. Elcoro, Jennifer Cano, M. G. Vergniory, Zhijun Wang, C. Felser, M. I. Aroyo, and B. Andrei Bernevig, Topological quantum chemistry, Nature (London) **547**, 298 (2017).
[46] M. I. Aroyo, J. M. Perez-Mato, Cesar Capillas, Eli Kroumova, Svetoslav Ivantchev, Gotzon Madariaga, Asen Kirov, and Hans Wondratschek, Bilbao crystallographic server: I. Databases and crystallographic computing programs, Z. Kristallogr. **221**, 15 (2006).
[47] Mois I. Aroyo, Asen Kirov, Cesar Capillas, J. M. Perez-Mato, and Hans Wondratschek, Bilbao Crystallographic Server. II. Representations of crystallographic point groups and space groups, Acta Crystallogr. Sect. A **62**, 115 (2006).
[48] Jian Kang and Oskar Vafek, Symmetry, Maximally Localized Wannier States, and a Low-Energy Model for Twisted Bilayer Graphene Narrow Bands, Phys. Rev. X **8**, 031088 (2018).

[49] Jennifer Cano, Barry Bradlyn, Zhijun Wang, L. Elcoro, M. G. Vergniory, C. Felser, M. I. Aroyo, and B. Andrei Bernevig, Topology of Disconnected Elementary Band Representations, Phys. Rev. Lett. **120**, 266401 (2018).

[50] Jennifer Cano, Barry Bradlyn, Zhijun Wang, L. Elcoro, M. G. Vergniory, C. Felser, M. I. Aroyo, and B. Andrei Bernevig, Building blocks of topological quantum chemistry: Elementary band representations, Phys. Rev. B **97**, 035139 (2018).

[51] Barry Bradlyn, Zhijun Wang, Jennifer Cano, and B. Andrei Bernevig, Disconnected elementary band representations, fragile topology, and Wilson loops as topological indices: An example on the triangular lattice, Phys. Rev. B **99**, 045140 (2019).

[52] Chen Fang, Matthew J. Gilbert, and B. Andrei Bernevig, Bulk topological invariants in noninteracting point group symmetric insulators, Phys. Rev. B **86**, 115112 (2012).

[53] Jian Kang and Oskar Vafek, Strong Coupling Phases of Partially Filled Twisted Bilayer Graphene Narrow Bands, Phys. Rev. Lett. **122**, 246401 (2019).

[54] B. Andrei Bernevig, Biao Lian, Aditya Cowsik, Fang Xie, Nicolas Regnault, and Zhi-Da Song, Twisted bilayer graphene. V. Exact analytic many-body excitations in Coulomb Hamiltonians: Charge gap, Goldstone modes, and absence of Cooper pairing, Phys. Rev. B **103**, 205415 (2021).

[55] B. Andrei Bernevig, Zhi-Da Song, Nicolas Regnault, and Biao Lian, Twisted bilayer graphene. III. Interacting Hamiltonian and exact symmetries, Phys. Rev. B **103**, 205413 (2021).

[56] Xiaoxue Liu, Zhi Wang, K. Watanabe, T. Taniguchi, Oskar Vafek, and J. I. A. Li, Tuning electron correlation in magic-angle twisted bilayer graphene using Coulomb screening, Science **371**, 1261 (2021).

[57] Oskar Vafek and Jian Kang, Towards the Hidden Symmetry in Coulomb Interacting Twisted Bilayer Graphene: Renormalization Group Approach, Phys. Rev. Lett. **125**, 257602 (2020).

[58] Justin H. Wilson, Yixing Fu, S. Das Sarma, and J. H. Pixley, Disorder in twisted bilayer graphene, Phys. Rev. Research **2**, 023325 (2020).

[59] Daniel E. Parker, Tomohiro Soejima, Johannes Hauschild, Michael P. Zaletel, and Nick Bultinck, Strain-Induced Quantum Phase Transitions in Magic Angle Graphene, Phys. Rev. Lett. **127**, 027601 (2021).

[60] Bikash Padhi, Apoorv Tiwari, Titus Neupert, and Shinsei Ryu, Transport across twist angle domains in moiré graphene, Phys. Rev. Research **2**, 033458 (2020).

[61] A. Uri, S. Grover, Y. Cao, J. Â. A. Crosse, K. Bagani, D. Rodan-Legrain, Y. Myasoedov, K. Watanabe, T. Taniguchi, P. Moon, M. Koshino, P. Jarillo-Herrero, and E. Zeldov, Mapping the twist-angle disorder and Landau levels in magic-angle graphene, Nature (London) **581**, 47 (2020).

[62] Nathanael P. Kazmierczak, Madeline Van Winkle, Colin Ophus, Karen C. Bustillo, Hamish G. Brown, Stephen Carr, Jim Ciston, Takashi Taniguchi, Kenji Watanabe, and D. Kwabena Bediako, Strain fields in twisted bilayer graphene, Nat. Mater. **20**, 956 (2021).

[63] Tjerk Benschop, Tobias A. de Jong, Petr Stepanov, Xiaobo Lu, Vincent Stalman, Sense Jan van der Molen, Dmitri K. Efetov, and Milan P. Allan, Measuring local moiré lattice heterogeneity of twisted bilayer graphene, Phys. Rev. Research **3**, 013153 (2021).

[64] Yarden Sheffer and Ady Stern, Chiral magic-angle twisted bilayer graphene in a magnetic field: Landau level correspondence, exact wave functions, and fractional Chern insulators, Phys. Rev. B **104**, L121405 (2021).

[65] Biao Lian, Zhi-Da Song, Nicolas Regnault, Dmitri K. Efetov, Ali Yazdani, and B. Andrei Bernevig, Twisted bilayer graphene. IV. Exact insulator ground states and phase diagram, Phys. Rev. B **103**, 205414 (2021).

[66] Biao Lian, Fang Xie, and B. Andrei Bernevig, Landau level of fragile topology, Phys. Rev. B **102**, 041402(R) (2020).

[67] Jian Kang, B. Andrei Bernevig, and Oskar Vafek, Cascades between Light and Heavy Fermions in the Normal State of Magic-Angle Twisted Bilayer Graphene, Phys. Rev. Lett. **127**, 266402 (2021).

[68] Gaurav Chaudhary, A. H. MacDonald, and M. R. Norman, Quantum Hall superconductivity from moiré Landau levels, Phys. Rev. Research **3**, 033260 (2021).

[69] Yuan Cao, Jeong Min Park, Kenji Watanabe, Takashi Taniguchi, and Pablo Jarillo-Herrero, Large Pauli limit violation and reentrant superconductivity in magic-angle twisted trilayer graphene, arXiv:2103.1208.

[70] Daniel Shaffer, Jian Wang, and Luiz H. Santos, Theory of Hofstadter superconductors, Phys. Rev. B **104**, 184501 (2021).

[71] Ipsita Das, Cheng Shen, Alexandre Jaoui, Jonah Herzog-Arbeitman, Aaron Chew, Chang-Woo Cho, Kenji Watanabe, Takashi Taniguchi, Benjamin A. Piot, B. Andrei Bernevig, and Dmitri K. Efetov, Observation of Reentrant Correlated Insulators and Interaction Driven Fermi-Surface Reconstructions at One Magnetic Flux Quantum per Moiré Unit Cell in Magic-Angle Twisted Bilayer Graphene, Phys. Rev. Lett. **128**, 217701 (2022).

[72] Yifei Guan, Oleg V. Yazyev, and Alexander Kruchkov, Re-entrant magic-angle phenomena in twisted bilayer graphene in integer magnetic fluxes, arXiv:2201.13062.